Egr2 upregulation induced mitochondrial iron overload implicating in sevoflurane-induced cognitive deficits in developing mice

Piao Zhang
Zhejiang University
Yeru Chen
Zhejiang University
Shuxia Zhang
Zhejiang University
Man Fang
Zhejiang University
Xianyi Lin
Zhejiang University
Tieshuai Liu
Zhejiang University
Youfa Zhou
Zhejiang University
Xin Yu
Zhejiang University
Gang Chen (chengang120@zju.edu.cn)
Zhejiang University https://orcid.org/0000-0002-8359-7417

Research article

Keywords: Sevoflurane, Cognitive dysfunction, Early growth response 2, Mitochondrial, Iron overload

Posted Date: December 22nd, 2020

DOI: https://doi.org/10.21203/rs.3.rs-131690/v1

Abstract

Background Sevoflurane inhalation initiated cognitive deficits implicated in mitochondrial dysfunction and synaptogenesis impairment. Bioinformatics analysis indicated that Egr2 may play a crucial role in maintaining cognitive function. Therefore, we attempted to clarify the potential mechanism regarding Egr2 expression and cognitive deficits induced by sevoflurane administration.

Methods Animals received sevoflurane anesthesia, and the behavioral tests including Morris water maze, novel object recognition test and trace fear conditioning were performed. Then, the immunofluorescent staining was employed to detect the effect of sevoflurane inhalation in hippocampal neurons. Meanwhile, bioinformatics analysis was implemented, and the level of lipid peroxidation, mitochondrial membrane potential, morphology and membrane permeability, and cytoplasm calcium levels were investigated after Egr2 interference by using JC-1 probe, MitoTracker staining, Mitochondrial permeability transition pore (mPTP) assay, and Fluo calcium indicators, respectively. Additionally, Prussian blue staining was used to evaluate the iron content.

Results The behavioral tests indicated that the cognitive function was significantly attenuated after sevoflurane administration. The Golgi-Cox staining displayed that the dendritic length, density and nodes were significantly reduced following sevoflurane inhalation. The bioinformatics analysis showed that sevoflurane administration results in the Egr2 expression upregulation. Additionally, the results suggested that sevoflurane administration elevated the cytoplasm calcium levels, reduced the mitochondrial membrane potential and triggered the opening of mPTP. Prussian blue staining showed that the iron deposition was apparently increased. However, Egr2 level downregulation partly reversed these above changes. Moreover, the behavioral performance was effectively improved after deferiprone (DFP) administration.

Conclusion These findings demonstrated that sevoflurane administration elicited mitochondrial dysfunction and iron dyshomeostasis, and eventually resulted in cognitive impairments, whereas suppressing Egr2 expression partly improved this pathological process.

Introductions

Cognitive dysfunction is one of the most serious complications threatening human health following anesthesia/surgery, which mainly characterized by memory and language deficits, visuospatial and executive dysfunctions, and behavioral disorders [1-3]. Generally, cognitive deficits would result in the loss of independence, a compromised quality of life and increased mortality, and thereby cause heavy economic and mental burden to the society and families [4]. Accumulating evidence revealed that anesthesia may provoke persistent abnormalities of neuronal circuits by affecting neuronal differentiation and synaptogenesis, and pharmacotoxic effects exacerbated the impairment of cognitive domains [5, 6]. Sevoflurane, as an inhaled volatile anesthetic agent, is widely used in pediatric practice [7]. Previous studies documented that multiple sevoflurane exposures in the neonatal period may induce a

long-lasting adverse impact including long-term behavioral abnormalities, and learning and memory deficits [8]. Sevoflurane administration triggers a series of pathophysiologic reactions comprising of mitochondrial dysfunction [9] and endoplasmic reticulum stress [10], and thereby results in cognitive deficits by initiating neuronal apoptosis [11], synaptogenesis impairment [12], and neuroinflammation [13].

Early growth response (EGR) genes are composed of four members (egr-1, egr-2, egr-3, and egr-4), which participate in synaptic and neuronal responses to external stimulation [14]. Of special note are that Egr2 facilitates robustly and sustainedly the maintenance of learning and memory by mediating the synaptic plasticity [15]. Meanwhile, related research suggested that Egr2 was involved in neural activity, synaptic transmission and nervous system development [16]. More interestingly, previous study indicated that the performance of motor learning and object recognition memory was enhanced in Egr2-deficient mice [17]. Mitochondrion, as a cellular organelle, participates in numerous bioenergetic, biosynthetic, and regulatory processes including oxidation-reduction reactions, DNA synthesis and repair [18]. Mounting evidence demonstrated that the dramatic morphological changes of mitochondria result in abnormal absorption and transport of iron, and thereby activate a serial cascade of inflammatory responses [19]. Furthermore, many intriguing studies showed that iron accumulation was closely correlated to the pathogenesis of neurodegenerative disorders including Alzheimer disease, Parkinson disease, and degenerative conditions [20]. Iron plays a crucial role in energy metabolism by mediating electron transport chain, ATP production and oxygen consumption [21]. However, excess iron in brain alters the behavior and mood [22], and causes the learning and memory deficits [23].

In this study, bioinformatics analysis indicated that Egr2 was closely correlated to the mitochondrial related genes, and jointly enriched in the same signal pathway with mitochondria. Therefore, we speculated that Egr2 may implicate in the maintenance of cognitive function by mediating mitochondrial function. Our findings revealed that sevoflurane inhalation induced the morphological alteration of mitochondria and iron metabolism abnormality, and consequently contributed to cognitive dysfunction associated with Egr2 elevation. These results were conduced to comprehensively illustrate the underlying mechanism and develop appropriate therapeutic strategy for attenuating cognitive deficits following sevoflurane administration.

Materials And Methods

Animals and Ethical statement

Neonatal C57BL/6 mice were purchased from Shanghai Laboratory Animal Center (Chinese Academy of Sciences, Shanghai, China). All experimental operations were in accordance with guidelines for laboratory animal care and safety from NIH, and approved by the Animal Care and Use Committee of Zhejiang University. All animals were housed with free access to water and chow in appropriate environmental conditions (temperature: 22-25℃, humidity: 45-50%, and 12 h light/dark cycle).

Experiment grouping and treatment

All animals were randomly assigned to different groups according to the experimental protocols: **Part1)** control group (Ctrl) and sevoflurane group (SEV); **Part2)** GFP-Ctrl group, GFP-SEV group, GFP-Egr2 shRNA-Ctrl group, GFP-Egr2 shRNA-SEV group; **Part3)** Ctrl group, SEV group, DFP group and SEV+DFP group. To induce general anesthesia, the pups were placed in an acrylic anesthetizing chamber with two interfaces including sevoflurane vaporizer and multi-gas monitor. The SEV group was exposed to 3% sevoflurane delivered in humidified 60% O_2 carrier gas for 2 h (2 L/min fresh gas for 3 min, followed by 1 L/min) by using the Datex-Ohmeda anesthesia system (Madison, WI, USA), while the Ctrl group received 60% oxygen (balanced with nitrogen) for the same period at postnatal day 6-8 (P6-8) [9]. Similarly, GFP-Ctrl group and GFP-Egr2 shRNA-Ctrl group received the same process with Ctrl group, and the GFP-SEV and GFP-Egr2 shRNA-SEV group underwent the scheme with SEV group. Moreover, to ensure sufficient ventilation, a single sample (100 μL) of arterial blood was obtained at the end of sevoflurane anesthesia or sham exposure by cardiac puncture from five mice of each group. These animals were not used for any other part of the study. Arterial carbon dioxide partial pressure ($PaCO_2$), arterial oxygen pressure (PaO_2), blood oxygen saturation (SaO_2) and power of hydrogen (pH) were evaluated by using a blood gas analyzer (Kent Scientific Corp., Torrington, CT, USA) (Table 1). There was no significant difference in pH, $PaCO_2$, PaO2, Glucose and SaO_2 level between the groups.

To downregulate Egr2 expression, transfection with adeno-associated virus was performed. Briefly, recombinant adeno-associated virus (AAV) was purchased from Vigene Biosciences company (Shangdong, China), which included either shRNA control (scrambled sequence) or Egr2 shRNA and enhanced green fluorescence protein (EGFP) gene. For Egr2 shRNA viral packaging, the shRNA sequence of mouse Egr2 (5'-GATCCGGGCAGGACAAAGCAATATTGTTCAAGAGACAATATTGCTTTGTCCTGCCCTTTTTTA-3') was synthesized and cloned into pAV-U6-GFP plasmid to produce pAV-U6-eGFP-Egr2 shRNA. Viral particles were purified by iodixanol step-gradient ultracentrifugation. The genomic titer was 4.72×10^{13} TU/mL determined by quantitative PCR. For viral injection, mice were anesthetized with ketamine (100 mg/kg) and xylazine (8 mg/kg) by intraperitoneal injection and placed in a stereotactic frame. Purified and concentrated lentivirus was injected bilaterally into the hippocampus (100 nL, coordinates from bregma − 1.5 mm anterior/posterior, − 2.07 mm medial/lateral, −1.8 mm dorsal/ventral) through glass micropipettes at a slow rate (10 nL/min). The GFP-Ctrl group and GFP-SEV group received AAV9-U6-shRNA(scramble)-GFP virus at P9, and the GFP-Egr2 shRNA group and GFP-Egr2 shRNA SEV group received AAV9-U6-Egr2 shRNA-GFP virus at P9, respectively.

To inhibit the level of iron, Deferiprone (DFP), an iron chelating agent [21], was administrated to detect the impact of iron chelating agent in mice after sevoflurane treatment. The mice in DFP group and SEV+DFP group were given Deferiprone (DFP) (100 mg/kg in 1% DMSO, i.p.) at P9 and the mice in Ctrl group and SEV group were given 50 μL of 1% DMSO by intraperitoneal injection at P9, respectively.

Behavioral test

Morris water maze

After the sevoflurane exposure, the spatial memory abilities were evaluated at P40 by using the Morris Water Maze (MWM) test as previously described [24]. A circular black pool (diameter: 120 cm; depth: 21 cm) was filled with opaque water using black non-toxic ink to reach 1.0 cm above the platform surface (diameter, 10 cm), and the water temperature was kept at 22 °C. Meanwhile, an invisible platform (diameter, 10 cm) was fixed in the pool and submerged 1 cm. In the training phase (P40-44), all animals received four training trials per day for a total of four days. The mice were placed into the pool at a random starting position and allowed to discover the hidden platform for 120 s. Mice were guided to the platform if they could not locate the platform within 2 min. The latency time (the time to reach the hidden platform) was recorded for assessing the spatial learning. In the testing phase (P45), the platform was removed, and the mean distance crossed the original platform site, platform-crossing times, and time spent were recorded for measuring memory function, respectively. After each trial, the mice were wiped dry and a heat lamp was used to faster temperature recovering before returning to home cages.

Novel object recognition test

Cognition was measured by the Novel object recognition (NOR) experiment at P35.

The animals are exposed to two identical objects for 20 min, then trained for 5 min during the familiarization phase. Thereafter, the mice are exposed to a single copy of the familiar object and a novel object (test phase) after 24h. The total distance traveled was recorded and the Recognition index was calculated [25]: A recognition index was calculated for each animal and re-ported as the ratio TB/(TA + TB), where TA = time spent exploring the familiar object A and TB = time spent exploring the novel object B. Recognition memory was evaluated as in the long-term memory test. Exploration was defined as sniffing or touching the object with the nose or forepaws.

Trace fear conditioning

The fear condition test is extensively used to detect the tone's effect on the hippocampus-dependent memory [26]. Briefly, the mice were placed in a sound attenuating fear-conditioning chamber (ACT-100A, Coulbourn Instrumnets, USA), The mice free explored for 2 min in the chamber, and the freezing was recorded as control. Then, the mice received 30s sound (80dB, 1500HZ) as conditioned stimulus, and foot shock (0.7 mA; 2 s) by the floor's steel rods at last 2 s, and keep the sound and the shock stopped at the same time. The mice stayed in the chamber for another 2 min. The training repeated for 5 times. The next day for contextual fear test, the mice were placed into the same chamber and the freezing was recorded for 5 min. After 2h, the mice were placed into another chamber for 3 min, then received the same conditioned stimulus for 3 min. The freezing of mice was recorded all the time. The data of freezing were recorded by Freeze Frame software.

Tissue harvest

Animals were anesthetized with 2% pentobarbital sodium (40 mg/kg, i.p.) at P42. Then, the right atrium was incised and transcardiac perfusion was performed with heparinized 0.9% saline followed by 4%

formaldehyde. The brain tissue was extracted and rinsed using 0.9% sodium chloride at 4 °C. The hippocampus was stripped and fixed in 30% sucrose in 0.1 M phosphate buffers (pH 7.4, 4 ℃) for 24-48h, then the specimens were stored in a −80 °C freezer.

TUNEL Assay

A TUNEL assay was performed to detect the DNA fragmentation caused by cell death in the hippocampus of aged rats. After preparation of sections (6 μm), the TUNEL staining was carried out using an in situ cell death detection kit (YEASEN, 40302ES20) according to the manufacturer instructions. Fluorescence signals were visualized under an epifluorescence microscope. Images were captured with the assistance of Image-Pro Plus 5.0 software, and all the parameters used in this experiment were kept consistent during capturing.

Immunofluorescent staining

Serial coronal slices (20 μm thick) of hippocampus including CA1, CA3 and DG regions were made by using a rotary microtome (Leica, Germany). The sections were placed in a water bath (96 °C, 20 minutes) for antigen retrieval and blocked using 10% bovine serum albumin at room temperature for 1 hour. The sections were incubated with antibody diluent containing goat antibodies against Tuj1 (1:500; Biolegnd, A488-435L), GFAP (1:100; ABclonal, A14673) and NeuN (1:1000; Abcam, ab104224) overnight at 4°C. Then sections were rinsed with PBS (3×10 min) followed by incubation with Alexa Fluor™ 488 goat anti-mouse antibody and Alexa Fluor™ 594 goat anti-rabbit antibody for 1 h at room temperature. After rinsing with PBS (6×5 min), fluorescence signals were visualized under an epifluorescence microscope. Images were captured with the assistance of Image-Pro Plus 5.0 software, and all the parameters used were kept consistent during capturing.

Golgi-Cox staining

The morphology of neuronal dendrites and dendritic spines was investigated in the hippocampus by using the Hito Golgi-Cox OptimStain^{TM} PreKit (Hitobiotec Corp. Kingsport, TN, USA). The brain tissues were obtained after sacrifice, and rinsed with Milli Q water. The equal volumes of Solutions A and B were used to impregnate the brain tissues, and the impregnation solution was replaced the following day and stored in darkness (Room temperature, 2 weeks). Then, the brain tissues were transferred to Solution C, which was replaced the following day. The brains were stored at 4 °C for 72 h in the dark. The Brain sections (100 μm thickness) were generated using a cryotome with the chamber temperature set at −19 °C. Each section was mounted on gelatin-coated microscope slides using Solution C. Each section was mounted on gelatin-coated microscope slides using Solution C. The excess solution on slide was removed using a Pasteur pipette and absorbed with filter papers, then the sections were allowed to dry naturally at room temperature for 3 days. The dried brain sections were processed according to the manufacturer's instructions. Thereafter, the dendrites of CA1 sub region in the hippocampus were observed by using an Olympus BX61 fluorescence microscope (Olympus, Japan).

RNA extraction

For the RNA-Seq analysis, the hippocampal tissues were obtained from Ctrl group and SEV group at P6 and P30, respectively. Total RNA was extracted from different group using RNAiso Plus Reagent (TaKaRa, Japan), and purified by RNasey Mini Kit (QIAGEN) based on the manufacturer's protocol. NanoDrop spectrophotometry (Thermo Scientific, Wilmington, USA) was used to detect the RNA concentration, and the integrity was confirmed through electrophoresis. Subsequently, the cDNA synthesis and antisense RNA (aRNA) amplification was performed using Amino Allyl MessageAmp II aRNA Amplification Kit (Ambion, USA). The total RNA was stored at -80°C for future use.

RNA-Seq

A total of 1.5 μg RNA was used as the input material. The clustering of the index-coded samples was performed by using a TruSeq PE Cluster Kit v3-cBot-HS (Illumina) based on the manufacturer's instructions. The library were sequenced using an Illumina HiSeq platform, and paired-end reads were generated followed by cluster generation. Thereafter, these raw reads in the fastq format were processed by using in-house Perl scripts. Low-quality data were discarded by using Trim Galore (http://www.bioinformatics.babraham.ac.uk/projects/trim_galore/). The GC-content and sequence duplication level of the clean reads were calculated, and the clean reads were assembled with Trinity software via the default parameters (https://github.com/trinityrnaseq/trinityrnaseq/wiki). Then, the RNA-seq data files were deposited in the NCBI Sequence Read Archive (SRA) database (SRA accession: Not uploaded, to date).

Data analysis by using integrated Differential Expression and Pathway analysis (iDEP) tools

The differentially expressed genes (DEGs) acquired from the RNA-seq-Based expression profiling were analyzed through iDEP (integrated Differential Expression and Pathway analysis) online tools (http://bioinformatics.sdstate.edu/idep/). To date, iDEP seamlessly connects 63 R/Bioconductor packages, 2 web services, and comprehensive annotation and pathway databases for 220 plant and animal species [27]. Briefly, the expression matrix of DEGs (Table S1 and Table S2) was filtered and converted to Ensemble gene IDs, and the exploratory data analysis (EDA) including K-means clustering and hierarchical clustering was performed using the pre-processed data. The pairwise comparison (Ctrl-6d group VS SEV-6d group; Ctrl-30d group VS SEV-30d group) was employed by using the DESeq2 package with a threshold of false discovery rate FDR < 0.05 and fold-change > 2. Additionally, a hierarchical clustering tree and network of enriched GO terms were constructed to visualize the potential connections among DEPs. Gene Set Enrichment Analysis (GSEA) method was used to investigate the related signal pathways activated by sevoflurane administration. Therefore, WGCNA was performed to construct co-expression networks and sub-modules, and the corresponding enriched pathways in selected module were exhibited, respectively.

Gene Ontology and KEGG Pathway Analysis of DEGs

Gene ontology (GO) analysis and Kyoto Encyclopedia of Genes and Genomes (KEGG) pathway were employed to analyze the differentially expressed genes (DGEs) between different groups (Ctrl-6d group VS SEV-6d group; Ctrl-30d group VS SEV-30d group) by using String online tools (https://string-db.org/cgi/input.pl). GO analysis was used to annotate genes and gene products including biological process (BP), cellular component (CC) and molecular function (MF). KEGG is utilized for systematic analysis of gene function and related high-level genome functional information of DGEs, which consists of a series of genome and enzymatic approaches and genomic information with higher order functional information [28].

Integration of Protein-Protein Interaction (PPI) Network Analysis and related database

STRING version 10.0 covers 9, 643, 763 proteins obtained from 2031 organisms [29]. The String database (https://string-db.org/cgi/input.pl) is used to predict the protein-protein interactions comprising direct/indirect associations. To investigate the potential relationships, String tool was constructed according to the function and pathway enrichment analysis. Moreover, the Genecards website (https://www.genecards.org) and The Human Protein Atlas database (https://www.proteinatlas.org/) were separately used to determine the expression of Egr2 in the tissues and organs of the human body.

Western blot

The hippocampal tissues, primary cultured neurons and cell lines among different groups were homogenized using RIPA buffer (Beyotime, P0013B) with 1 × protease inhibitor cocktail (Beyotime, P1010). The supernatant was collected by centrifugation (16, 200×g, 10 min), and the protein concentration was measured through a bicinchoninic acid protein assay kit (Beyotime, P0012S). An aliquot of 50 μg protein was separated via SDS-PAGE and transferred to a nitrocellulose membrane, then blocked with 5% nonfat milk in phosphate-buffered saline (PBS, pH 7.4). The membranes were incubated with primary antibodies against Egr2 (1:1, 000; ABclonal, A15053), ACSL4 (1:500; ABclonal, A16848), FTH1 (1:500; ABclonal, A19544), GPX4 (1:1, 000; abcam, ab125066), COX2 (1:1,000; ABclonal, A1253), DRP1 (1:500; ABclonal, A17069), DMT1 (1:500; ABclonal, A10231), Ferroportin-1 (1:1, 000; abcam, ab78066, actin (1:5, 000; ABclonal, AC026) at 4 °C overnight. Blots were incubated in horseradish peroxidase-conjugated secondary antibodies against rabbit IgG (1:5, 000, CST, 7071 and 7072) for 2 h at room temperature, then subjected to chemiluminescent detection using the SuperSignal West Pico Substrate (34077, Pierce) and exposed to film. Digital images were quantified using densitometric measurements obtained using Quantity One software (Bio-Rad).

Cell culture

Primary hippocampal neurons were cultured by using fetal mice (E17) hippocampi according to a previously described protocol [30]. Briefly, the mice pregnancy for 17 days was anesthetized through 1% isoflurane, and the uterus was exposed and the fetus was removed. The fetal mice were sacrificed and the hippocampi were obtained under a sterile environment. Then, the hippocampi were treated using 0.125% trypsin in Hank's buffer (in mmol/L: 137 NaCl, 5.4 KCl, 0.4 KH_2PO_4, 0.34 $Na_2PO_4 \cdot 7H_2O$, 10

glucose and 10 HEPES) for 12 min at 37 °C and dissociated by repeated passage with Pasteur pipettes. The nerve cells ($2 \times 10^5/cm^2$) were seeded onto poly-l-lysine (10 μg/mL)-coated plates added culture reagents including Neurobasal Medium (Invitrogen), 2% B27 (Invitrogen), 10 U/mL penicillin, 10 U/mL streptomycin, and 0.5 mmol/L glutamine. Hippocampal neurons were cultivated in appropriate environment (37 °C, 5% CO_2). The cells were continuous cultured for 20 d, then harvested for subsequent experiments. Moreover, the cell lines consisting of H4 human neuroglioma were obtained from the China Center for Type Culture Collection. These cells were cultured using Dulbecco's Modified Eagle's Medium (DMEM) supplemented with 10% F12 (all from Gibco, Grand Island, NY, USA) and 10% heat-inactivated fetal bovine serum in a humidified incubator (37 °C, 5% CO_2).

Sevoflurane treatment

The cultured cells were placed in an airtight plastic chamber (MIC-101), which was connected to an acrylic anesthetizing chamber with two interfaces including a sevoflurane vaporizer and a multi-gas monitor. The chamber was gassed with 4.1% sevoflurane in the carrier gas (95% air/5% CO_2) for 15 min, and the concentration of sevoflurane was monitored by a gas monitor (PM 8060, Drager, Lübeck, Germany) [31]. Then, the chamber was sealed and incubated for 6 h at 37 °C. The gas was renewed every 3 h, and the concentration of sevoflurane was confirmed at the end of the incubation. Meanwhile, the control group received the same procedure with air containing 5% CO_2.

Plasmid and transfection

pAU-U6-shRNA (Egr2) plasmid was purchased from Vigene Biosciences (Shandong, China). pAU-U6-shRNA (Egr2) plasmid used the shRNA sequence: GGGCAGGACAAAGCAATATTGTTCAAGAGACAATATTGCTTTGTCCTGCCCTTTTTT. The plasmids pAU-U6-shRNA (Egr2) was transfected into H4 cells using Lipofectamine 3000 reagent following the specific protocol for this cell line.

Iron Levels detection

Iron assay was performed according to the manufacturers' protocol of Iron Assay Kit (Abcam, ab83366) [32]. Briefly, the specimens were incubated with iron reducer at 25 °C for 30 min followed by incubating for 60 min with iron probe at 25 °C. Then, the microplate reader (OD 593 nm) was used to detect the level of iron.

Lipid peroxidation assay

To detect the level of lipid peroxidation, the fluorescent reporter molecule C11-BODIPY$^{581/591}$ (Invitrogen^{TM}, D3861) was used. Cells were induced with the probes for 30 min (2.5 μM), and the fluorescence of C11-BODIPY$^{581/591}$ shifted from red to green. The fluorescence spectrophotometer was utilized to monitor this kinetics of the reaction, and the fluorescence emission intensity at 520 nm was

recorded. Images were captured with the assistance of Image-Pro Plus 5.0 software, and all the parameters used were kept consistent during capturing.

Detection of mitochondrial membrane potential and calcium level

Mitochondrial membrane potential was detected by using JC-1 (Thermo Fisher Scientific, MA, USA) fluorescent dye. H4 cells were randomly divided into four groups including Ctrl group, SEV group, Egr2 shRNA group and SEV+ Egr2 shRNA group, and these cells were cultured for 6 h. Then, 10 μM JC-1 reagent was added and stained for 20 min. JC-1 emits fluorescence including red fluorescent J-aggregates (530 nm excitation/590 nm emission) at high potentials, and green fluorescent J-monomers (490 nm excitation/530 nm emission) at low potentials. The cells were visualized immediately after treatment using an epifluorescence microscope. Images were captured with the assistance of Image-Pro Plus 5.0 software.

Additionally, the cytoplasmic calcium level was measured using Fluo calcium indicators (Fluo-4, AM, YEASEN, 40704ES50). An aliquot of DMSO stock solution (5 mM) was diluted to a final concentration of 5 μM in buffered physiological medium. H4 cells were washed with indicator-free medium after treating for 6 h. The fluo acetoxymethyl ester was used for cell incubation (30-60 min, 37°C). Cells were washed in indicator-free medium once again prior to fluorescence was measured. The fluorescence signals were visualized by an epifluorescence microscope after treatment. Images were obtained with the assistance of Image-Pro Plus 5.0 software.

MitoTracker Imaging

H4 cells were randomly divided into four groups consisting of Ctrl group, SEV group, Egr2 shRNA group and SEV+Egr2 shRNA group, and these cells received corresponding treatment for 6 h. The medium was replaced with pre-warmed (37°C) 50 nM MitoTracker (Invitrogen) medium for 10 min. Thereafter, the loading solution was replaced with fresh medium once again. The cells were visualized after treatment by using an epifluorescence microscope. Images were captured with the assistance of Image-Pro Plus 5.0 software.

Mitochondrial permeability transition pore assay

Mitochondrial transition pore assay kit (C2009S, Beyotime, China) was used to visualize the mitochondrial transition pores according to the manufacturer's instructions. Cells were stained using acetoxymethyl ester of calcein dye (calcein AM, green) followed by incubating with CoCl2 solution, which effectively quenched the calcein fluorescence in the cytoplasm. The calcein fluorescence could not be quenched if the MPTP is tightly closed, while the $Co2^{+}$ ions enter the mitochondria to quench the mitochondrial calcein fluorescence when the MPTP is open. Mitochondrial pore opening reduced the green fluorescence.

Determination of Malondialdehyde (MDA) and GSH Levels

Tissue proteins were prepared as described in the Lipid Peroxidation MDA assay kit (Beyotime, S0131). The MDA concentration of each sample was evaluated by multimode microplate readers (SpectramMax M5) at 532 nm, and using 490 nm served as a control. Additionally, the level of GSH were measured according to the requirements of the instructions in reagent kits (Beyotiome, S0052), and the protein concentration was determined with BCA protein assay reagent kit. The values were normalized to total protein in tissue samples.

Reactive oxygen species determination

H4 human neuroglioma cells were randomly divided into four groups including Ctrl group, SEV group, Egr2 shRNA group and SEV+ Egr2 shRNA group, and the regional mitochondrial ROS accumulation was measured by using the Mito-SOX reagent (M36008, Thermo Fisher, USA). After treatment, H4 cells were washed with HBSS solution buffer. A 5 μM Mito-SOX working solution was then prepared. Next, 1.0 mL of the 5 μM Mito-SOX reagent was applied as a cell loading solution in which cells were incubated for 10 min at 37 °C without light exposure. Cells were then gently washed three times with warm PBS. Excitation wavelengths were measured at 510 nm and emission at 580 nm by a fluorescence microplate reader (SpectraMax M5/M5e). The intracellular ROS levels in H4 cells were measured with the fluorescent probe dihydroethidium (DHE). After being treated with 4.1% sevoflurane for 6 h, H4 cells were incubated with 1 μM DHE (YEASEN, 50102ES02, China) for 60 min at 37°C. Excitation wavelengths were measured at 518 nm and emission at 610 nm by a fluorescence microplate reader (SpectraMax M5/M5e).

Mitochondrial respiration analysis

The oxygen consumption rate (OCR) was measured by using a Seahorse XF96 analyzer (Seahorse Agilent, USA) combined with the Agilent Seahorse XFe96 Extracellular Flux Assay Kit according to the manufacturer's recommendations. Briefly, H4 cells were seeded in 96-wells of a Agilent Seahorse XF96 cell culture microplate (101085-004) and received corresponding treatment for 6 h. The culture medium was replaced with 175 μL assay medium, supplemented with 25 mM glucose, 2 mM glutamine, and 2 mM pyruvate on the day of the assay. Prior to the assay, plates were incubated at 37°C for approximately 1 h in a non-CO2 incubator. Afterwards, the basal OCR was determined followed by the automated injection of 25 μl oligomycin (8 μM), and mixing for 3 min and measurement for 2 min. Next, 25 μl carbonyl cyanide 4-(trifluoromethoxy) phenylhydrazone (FCCP) (9 μM) was injected, and OCR was measured for 2 min. Finally, a combination of 25 μl rotenone (20 μM) + antimycin A (100 μM) was injected, followed by the same mixing and measurement steps. ECAR was automatically recorded by the Seahorse XFe96 software, and the respiration rate was calculated by the Seahorse analyzer.

MitoTracker and ERTracker Imaging

H4 cells were randomly divided into four groups (Ctrl group, SEV group, Egr2 shRNA group and SEV+ Egr2 shRNA group), and these cells received corresponding treatment for 6 h. Thereafter, the medium was replaced with prewarmed (37 °C) MitoTracker medium (50 nM, Invitrogen) for 5 min and ERTracker medium (100 nM, invitrogen) for 30 min. cells were permeabilized with 0.2% Triton® X-100 for 10

minutes and incubated with antibody diluent containing goat antibodies against Drp1 (1:100; ABclonal, A17069) overnight at 4 °C. Then sections were rinsed with PBS (3×10 min) followed by incubation with Alexa Fluor™ 594 goat anti-rabbit antibody for 1 h at room temperature. After rinsing with PBS (6 × 5 min), fluorescence signals were visualized under an epifluorescence microscope. Images were captured with the assistance of Image-Pro Plus 5.0 software, and all the parameters used were kept consistent during capturing.

Morphological observation of mitochondria

The hippocampal tissues were fixed with 2.5% glutaraldehyde overnight at 4 °C, and post-fixed with 1% osmium tetraoxide for 2 h after rinsing for three times with phosphate-buffered saline (PBS). Then, the specimens were rinsed with distilled water followed by a graded ethanol dehydration series ending with propylene oxide. After infiltration in a mixture of one-half propylene oxide and one-half resin, the tissues were embedded in resin. Cross sections (120 nm) were made, which were stained with 4% uranylacetate for 20 min and 0.5% lead citrate for 5 min. The morphology of mitochondria in the hippocampal neurons was observed by using a transmission electron microscope (TEM) (Phliphs Tecnai 10, Holland) in the Center of Cryo-Electron Microscopy at Zhejiang University.

Prussian blue staining

Sections (5 μm) were stained for Prussian blue reaction through an Iron Stain Kit (YEASEN, 60533ES20) according to the manufacturer's instructions. Briefly, slides were deparaffinized and hydrated to deionized water. Then, the samples were immersed in a freshly prepared solution of equal parts 5% potassium ferrocyanide and 5% hydrochloric acid for 10 min. Meanwhile, the samples were rinsed using deionized water, immersed in 2% pararosaniline solution for 5 min, and rinsed with deionized water once again, and immediately dehydrated and coverslipped. Images of positively stained sections were captured via an Olympus BX61 microscope.

Statistical analysis

SPSS 19.0 software was used to process the data. All data are represented as mean ± standard deviation, and analyzed by one-way analysis of variance (ANOVA) and Tukey's post hoc test. $P<0.05$ was considered statistically significant.

Results

Sevoflurane Exposures induced Cognitive Impairment in developing mice

To determine the effect of sevoflurane administration on cognitive function, behavioral tests including Morris Water Maze, novel object recognition test and trace fear conditioning were performed. Briefly, animals were exposed to 3% sevoflurane for 2 h at P6-P8. Cognition was measured by the Novel object recognition (NOR) experiment at P30.The spatial memory abilities were evaluated at P37 by using the Morris Water Maze (MWM) test. And auditory trace fear conditioning, as a hippocampus-dependent

learning task, was performed at P30. The results showed that the time course of mean escape latency was longer at third and fourth day in SEV group than that of in Ctrl group (Fig. 1A, $P < 0.05$). The time spent in the target quadrant and the total number of platform area crossings were significantly decreased in SEV group compared to Ctrl group (Fig. 1B-D, $P < 0.05$). The fear condition test showed that the freezing time was dramatically reduced in SEV group than that of in Ctrl group (Fig. 1E-G, $P < 0.05$). The novel object recognition test suggested that the overall distance of traveling was no significant different (Fig. 1H, $P > 0.05$), while the recognition index was decreased in SEV group compared to Ctrl group (Fig. 1I, $P < 0.05$).

Sevoflurane administration induced the neuronal death and reduced the synapse formation in hippocampus

The hippocampal tissues of mice were harvested at P42 after sevoflurane administration at P6-P8, and the immunofluorescence staining was performed. The results showed that the relative fluorescence intensity of Tuj1 were obviously increased, while the GFAP and NeuN fluorescence intensity were decreased in SEV group including DG, CA1 and CA3 region compared to Ctrl group (Fig. 1J, K, M, N; $P < 0.05$). The TUNEL assay was used to visualize the apoptosis, and the results showed that the apoptotic cells were significantly increased in SEV group than that of in Ctrl group (Fig. 1L, O; $P < 0.05$). Meanwhile, the results displayed that the dendritic length, density and nodes were significantly reduced after sevoflurane administration compared with Ctrl group indicated by Golgi-Cox staining (Fig. 1P, Q; $P < 0.05$).

Bioinformatics analysis indicated that Sevoflurane administration resulted in the Egr2 expression significantly upregulated

The hippocampal tissue of mice was obtained at P30 after sevoflurane treatment, and the RNA-Seq was performed. Then, to further clarify the potential mechanism, the data were analyzed by using integrated Differential Expression and Pathway analysis (iDEP) tools and String database. The results showed that the differential expression genes (DEGs) including 3 upregulated and 18 downregulated genes were screened by using IDEP tools with FDR < 0.05, Fold Change > 2 (Fig. 2A), and these genes were enriched in various signal pathways consisting of learning or memory (Fig. 2B). Then, these hub genes were further analyzed through String database. Briefly, the GO function analysis as a dynamic controlled vocabulary is utilized to describe the role of gene with three categories information comprising of biological process (BP), cellular component (CC), and molecular function (MF). GO term enrichment analysis indicated that the BP was involved in 88 categories, and the top 10 BP was presented in Fig. 2C; the CC consists of 2 categories showed in Fig. 2D; and the MF includes 17 categories, and the top 10 MF was showed in Fig. 2E. The PPI network analysis was constructed for DEGs, and the results were showed in Fig. 2F, and the volcano plot showed the distribution of DEGs according to the Fold Change and *P* value (Fig. 2G, Table S3). Meanwhile, the bubble diagram showed the enriched pathways of DEGs (Fig. 2H). Gene coexpression was visualized by String tools, which revealed that Arc and Egr2 were coexpression in human beings and Mus nusculus (Fig. 2I), and may participated in the regulation of synapse formation [33, 34]. Moreover, the genes related cognitive function and mitochondrial function were analyzed by

String and KEGG database, and the results displayed that the genes mediating cognitive function were closely correlated to the mitochondrial related genes, and enriched in the same signaling pathway (Fig. 2J, K). Additionally, the Genecards database (https://www.genecards.org) was used to search the mRNA expression in normal human tissues from GTEx, Illumina, BioGPS, and SAGE (Serial Analysis of Gene Expression) for Egr2 Gene. Meanwhile, The Human Protein Atlas website (https://www.proteinatlas.org/) was utilized to retrieve this Egr2 expressional data separately obtained from Consensus Human Brain Dataset, GTEx Human Brain RNA-Seq Dataset and FANTOM5 Human Brain CAGE Dataset. And the results showed that the expression level of Egr2 was low specially in hippocampal formation (Fig. 2N-Q). The RNA-Seq results showed that the expression level of Egr2 was significantly upregulated in SEV group compared to Ctrl group at P6 and P30 (Fig. 2L). Similarly, the WB results indicated that the relative protein level of Egr2 was significantly increased in SEV group when compared with Ctrl group in animal hippocampus and primary cultured neuron, respectively (Fig. 2M, $P < 0.05$). These above data suggested that Egr2 played a vital role in sevoflurane-induce cognitive dysfunction in developing mice.

Egr2 downregulation alleviated the cognitive deficits induced by sevoflurane administration in developing mice

To determine the effect of Egr2 downregulation in cognitive function, the recombinant adeno-associated virus (AAV) was transfected into the hippocampus by intracerebroventricular injection assisted with stereotaxic apparatus. Six-day-old mice received anesthesia with 3% sevoflurane 2 hours daily on postnatal days 6, 7, and 8. The mice were received Egr2 shRNA at P9 and sacrificed at P42 after behavior detection. The green fluorescence suggested that the AAV successfully reached the ventricular injection sites (Fig. 3J). Then, the WB assay was performed and the results showed that the Egr2 protein level was significantly elevated in GFP-SEV group than that of in GFP-Ctrl group (Fig. 3K, $P < 0.05$). Whereas, the Egr2 protein level was obviously reduced in GFP-Egr2 shRNA-SEV group compared to GFP-SEV group (Fig. 3K, $P < 0.05$). Meanwhile, the behavioral tests including Morris Water Maze, novel object recognition test and trace fear conditioning were performed. The results showed that there were no significant different among the time course of mean escape latency, the time spent in the target quadrant and the total number of platform area crossings in GFP-Egr2 shRNA-Ctrl group when compared with GFP-Ctrl group (Fig. 3A-C; $P > 0.05$). However, the time course of mean escape latency was reduced at third and fourth day (Fig. 3A; $P < 0.05$), and the time spent in the target quadrant and the total number of platform area crossings were obviously increased in GFP-Egr2 shRNA-SEV group when compared with GFP-SEV group (Fig. 3B, C, I; $P < 0.05$). The memory retrieval test showed that the freezing time was significantly increased in GFP-Egr2 shRNA-SEV group compared to GFP-SEV group (Fig. 3D-F; $P < 0.05$). The novel object recognition test displayed that the recognition index was reduced in GFP-SEV group when compared to GFP-Ctrl group, while which was increased in GFP-Egr2 shRNA-SEV group compared with GFP-SEV group (Fig. 3H, $P < 0.05$). Moreover, the results of Golgi-Cox staining indicated that the dendritic length, density and nodes were significantly increased in GFP-Egr2 shRNA-SEV group compared to that of in GFP-SEV group (Fig. 3L).

Egr2 downregulation partly improved mitochondrial dysfunction induced by Sevoflurane administration

Mitochondria are the cellular structures responsible for energy metabolism, and participate in various cellular biological processes. Previous study suggested that sevoflurane inhalation may result in mitochondrial dysfunction by inducing reactive oxygen species formation [35]. Bioinformatic analysis displayed that Egr2 was closely correlated to the mitochondrial related genes, and enriched in the same signaling pathway associated with mitochondria (Fig. 2J, K). In this study, the mitochondrial membrane potential, morphology, membrane permeability and cytoplasm calcium level were detected in H4 cells by using JC-1 probe, MitoTracker staining, mitochondrial permeability transition pore (mPTP) assay and Fluo 4-AM calcium indicators, respectively. Meanwhile, the mitochondrial ultrastructure was observed by cryo-SEM, and the MDA and GSH level was measured in hippocampal tissues. Additionally, the OCR was evaluated and ECAR was automatically recorded by using a Seahorse XF96 analyzer to determine the respiration rate in H4 cells by using the Seahorse analyzer. The results of mitochondrial membrane potential showed that the red fluorescence was decreased and green fluorescence was increased in SEV group compared with Ctrl group (Fig. 4A, B; $P < 0.05$). Whereas, the red fluorescence was increased and green fluorescence was decreased in SEV + Egr2 shRNA group compared with SEV group (Fig. 4A, B; $P < 0.05$). Mitochondrial morphology was detected by MitoTracker staining and cryo-SEM, and the representative imaging showed that sevoflurane administration accelerated the formation of fragmentation, reduced volume, intercristal space, and length in mitochondria compared with Ctrl group, while this status was partly reversed in SEV + Egr2 shRNA group when compared to SEV group (Fig. 4A, E; $P < 0.05$). mPTP assay was employed to detect the membrane permeability by observing the fluorescence quenching. The results showed that the green fluorescence was reduced in SEV group than Ctrl group, whereas which was effectively enhanced in SEV + Egr2 shRNA group compared with SEV group (Fig. 4A, C; $P < 0.05$). Meanwhile, the Fluo 4-AM calcium indicators displayed that the cytoplasm calcium levels were upregulated in SEV group compared to Ctrl group, while which was downregulated in SEV + Egr2 shRNA group compared with SEV group (Fig. 4A, D; $P < 0.05$). Moreover, the results showed that the concentration of MDA in hippocampus was no significant different between GFP-Egr2 shRNA-Ctrl group and GFP-Ctrl group, but which was obviously decreased in GFP-Egr2 shRNA-SEV group compared to GFP-SEV group (Fig. 4F, $P < 0.05$). Similarly, the level of GSH of hippocampuswas decreased in SEV group than Ctrl group, but which was effectively evaluated in SEV + Egr2 shRNA group compared to SEV group (Fig. 4G, $P < 0.05$). Additionally, the DHE and mito-SOX staining were used to detect the level of intracellular and mitochondrial ROS in H4 cells, respectively. The data suggested that sevoflurane administration obviously enhanced the the intracellular ROS level and the mitochondrial ROS level, while Egr2 gene silencing effectively reversed the ROS level in intracellular and mitochondrial compared with SEV group (Fig. 4H, $P < 0.05$). Furthermore, the OCR and ECAR assay were separately performed to investigate the mitochondrial respiratory function including anaerobic glycolysis and aerobic respiration in H4 cells. Sevoflurane administration significantly suppressed mitochondrial respiration consisting of reducing aerobic respiration and enhancing anaerobic glycolysis (Fig. 4I, J). Particularly, the ATP production, basal respiration and maximum respiration were obviously decreased in SEV group than Ctrl

group, whereas which were significantly elevated in SEV + Egr2 shRNA group compared with SEV group (Fig. 4K-M, $P < 0.05$).

Egr2 downregulation alleviates iron overload-induced ER-mediated mitochondrial fission in hippocampal primary neurons

The mitochondrial deficits would elicit metabolic disequilibrium and eventually result in neurogenetic abnormal. Accumulating evidence revealed that mitochondria was closely correlated to iron homeostasis [36]. To investigate the interrelation between mitochondria dysfunction and iron homeostasis, the related protein and iron content were detected in H4 cells and hippocampal tissues. The results showed that the protein level of ACSL4 and COX2 was upregulated, but the GPX4 and FTH1 protein level was downregulated in SEV group compared with that of in Ctrl group (Fig. 5A). Meanwhile, the protein level of ACSL4 and COX2 was upregulated, while the GPX4 and FTH1 protein level was downregulated in GFP-Egr2 shRNA-SEV group compared with GFP-Ctrl group in neuron and hippocampus, respectively (Fig. 5B, C). Whereas, the protein level of ACSL4 and COX2 was reduced, while the GPX4 and FTH1 protein level was increased in GFP-Egr2 shRNA + SEV group compared to that of in GFP-SEV group in neuron and hippocampus, respectively (Fig. 5B, C). The iron assay showed that sevoflurane administration significantly induced iron overload compared to Ctrl group in animal hippocampus (Fig. 5D, $P < 0.05$). However, the iron content was reduced in GFP-Egr2 shRNA-SEV group compared to that of in GFP-SEV group in animal hippocampus (Fig. 5E, $P < 0.05$). Meanwhile, iron distribution was assessed histologically in hippocampus of animals by using Perls' Prussian blue staining. The results showed that the iron deposition was apparently elevated in SEV group than Ctrl group, but which of in SEV + Egr2 shRNA group were effectively reversed when compared to SEV group (Fig. 5H). To detect the level of lipid peroxidation, the fluorescent reporter molecule C11-BODIPY$^{581/591}$ was employed in primary cultured neurons. The results showed that the fluorescence partly shifted from red to green after sevoflurane administration (Fig. 5G). The quantitative results showed that the red fluorescence was decreased and green fluorescence was increased in SEV group compared with that of in Ctrl group (Fig. 5G, K; $P < 0.05$). However, the red fluorescence was increased and green fluorescence was decreased in SEV + Egr2 shRNA group compared to SEV group (Fig. 5G, K; $P < 0.05$).

Moreover, to investigated the correlation between Egr2 expression and iron overload-induced mitochondrial fission, the immunofluorescence co-localization analysis including MitoTracker (Red), ERTracker (Green), and Drp1 (Blue) were employed in hippocampus. The results showed that sevoflurane administration induced iron overload, and thereby increases the co-localization of Drp1 puncta and expanded ER on mitochondria/fragmented mitochondria in hippocampal neurons when compared with Ctrl group; whereas, the co-localization among Drp1 puncta, expanded ER, and mitochondria/fragmented mitochondria was effectively reduced in SEV + Egr2 shRNA group than SEV group (Fig. 5F, J; $P < 0.05$). Additionally, the WB assay was performed for detecting iron metabolism and mitochondrial fission-related proteins, and the results showed that the protein level of DRP1, DMT1 and Ferroportin-1 was upregulated in SEV group than that of in Ctrl group, while which was downregulated in SEV + Egr2 shRNA group when compared with SEV group (Fig. 5I, $P < 0.05$).

The Behavioral Performance Was Effectively Improved After Deferiprone Administration

To investigate the effect of iron overload on cognitive deficits following sevoflurane inhalation, the deferiprone (DFP) was administrated to evaluate the impact of iron chelating agent in mice after sevoflurane treatment. Six-day-old mice received anesthesia with 3% sevoflurane 2 hours daily on postnatal days 6, 7, and 8. The mice received deferiprone at P9 and were sacrificed at P42 after Morris Water Maze test. The results of Morris Water Maze showed that the time course of mean escape latency was increased in SEV group than Ctrl group, while which was reduced in SEV + DFP group compared with SEV group at third and fourth day (Fig. 6A; $P < 0.05$). The time spent in the target quadrant and the total number of platform area crossings were obviously decreased in SEV group when compared with Ctrl group, but these of increased in SEV + DFP group compared to SEV group (Fig. 6B-D; $P < 0.05$). Meanwhile, the hippocampus was harvested for the iron content detection and western immunoblotting assay. The iron assay indicated that sevoflurane administration significantly induced iron overload compared with Ctrl group in animal hippocampus (Fig. 6E, $P < 0.05$). Whereas, the iron content was reduced in SEV + DFP group than SEV group in animal hippocampus (Fig. 6E; $P < 0.05$). Moreover, the WB assay showed that the protein level of ACSL4 and Cox2 was significantly increased in SEV group than Ctrl group, while which was reduced in SEV + DFP group when compared to SEV group (Fig. 6F; $P < 0.05$). And the protein expression of FTH1 and GPX4 was decreased in SEV group than Ctrl group, while which was elevated in SEV + DFP group compared with SEV group (Fig. 6F; $P < 0.05$)

Discussion

Cognitive dysfunction is a common complication involving in learning and memory deficits, attention and information processing anomalies, and personality and social ability disorders [37, 38]. Related researches revealed that anesthesia accelerated the formation of extracellular amyloid plaques and intraneuronal neurofibrillary tangles, elevated the generation and accumulation of Aβ, and subsequently exacerbates neurofibrillary degeneration and induced nerve impairment [39]. Meanwhile, previous studies documented that anesthesia inhalation would result in direct toxic effects in neurons by inducing the dysregulation of calcium homeostasis and neurotransmitter release, aggravating the endogenous neurodegeneration processes, and inhibiting the physiological functions of neural stem cells [40]. Currently, sevoflurane was extensively used in pediatric practice as an inhaled volatile anesthetic agent. Emerging evidence demonstrated that sevoflurane administration induced the neuroinflammation and neuronal damage, reduced the synaptic plasticity, and eventually resulted in cognitive impairment [41]. In this study, our results showed that the the learning and memory performance were significantly impaired following sevoflurane inhalation in developing mice. Immunofluorescent staining displayed that the immature neurons were increased and the mature neurons were reduced in hippocampus. Golgi-Cox staining displayed that the dendritic length, density and nodes were obviously reduced after sevoflurane administration. Most intriguingly, bioinformatics analysis showed that the Egr2 expression was significantly elevated, and closely correlated to mitochondrial function. Thereafter, the level of lipid peroxidation, mitochondrial membrane potential, morphology and membrane permeability, and cytoplasm calcium levels were investigated after Egr2 expression silence, respectively. Our results provide

abundant evidence for clarifying the underlying mechanism regarding the cognitive dysfunction induced by sevoflurane administration, which implicated in destroying mitochondrial respiratory network, elevating mitochondria ROS and reducing membrane potential, disturbing calcium homeostasis and iron content, and eventually resulting in cognitive deficits.

Mitochondria, as one of the chief sources of reactive oxygen species (ROS), play a crucial role in maintaining normal physiological activities. Excessive stimulation of NAD(P)H and electron transport chain would disrupt the normal redox state of cells and cause the overproduction of peroxides and free radicals, and thereby lead to the oxidative damage and mitochondrial dysfunction [42]. Meanwhile, the mitochondrial DNA impairment derived from accumulation of superoxide radicals would further amplify oxidative stress by mediating critical proteins, and initiating a vicious circle of ROS production to destroy the organelle, induce metabolic disequilibrium and genomic instability, and eventually result in cognitive impairment [43–45]. Hippocampus is one of the most vulnerable brain regions to oxidative damage, which is critical for the formation of long-term memory and learning [46]. Previous studies showed that Egr2 was intimately connected with the formation of myelination [47]. Egr2 expression was reduced after microneme-mediated attachment was blocked using a calcium chelator [48]. Meanwhile, Egr2 may participate in increasing adipocyte mitochondrial respiration and dampening oxidative stress reaction [49]. In this study, bioinformatics analysis revealed that Egr2 may implicate in the mitochondrial metabolic process. And the results showed that sevoflurane administration accelerated the formation of fragmentation, reduced volume and intercristal space, elevated the intracellular ROS level in hippocampal mitochondria, and consequently resulted in the impairment of behavioral outcomes. Interestingly, we found that Egr2 expression silencing could effectively reverse the elevation of cytoplasm calcium content, reduction of the mitochondrial membrane potential and the opening of mPTP following sevoflurane administration.

Iron is a crucial component for biochemical reactions including cellular metabolism, synthesis of DNA, RNA and proteins, enzymatic reactions, and synthesis of myelin [50]. Accumulating evidence revealed that neurons were particularly vulnerable to the alteration of iron content, and iron homeostasis disorder triggers a serial cascade of pathophysiologic reactions including neurogenetic abnormality, disturbing neurotransmitter synthesis and release, and mitochondrial dysfunction [51]. Previous studies showed that iron participated in the generation of ROS, and caused aggregation and phosphorylation of tau, and thereby aggravated the toxicity by mediating DNA oxidation, lipid peroxidation, accumulation of advanced glycation end products, malondialdehyde and peroxynitrite in Alzheimer patients [52]. Recently, related research proved that sevoflurane disrupted iron homeostasis by affecting the protein expression and mitochondrial iron accumulation [53]. Mitochondria are major generators of iron-sulfur clusters (ISC), and tightly regulated iron uptake and utilization [54]. Additionally, mitochondrion could effectively catalyze electron transport through heme- and ISC -containing proteins to process energy transduction owing to the reversible oxidation states of iron. The prevailing hypothesis indicated that the mitochondrial iron content was affected by the labile iron pool in the cytosol, and Fe^{2+} was transported into the mitochondria by binding with hydrophobic pockets of chaperone proteins [55]. Meanwhile, Egr2

gene may correlated with the HO-1 expression, which could convert heme to iron, and participated in memory, cognition and synaptic plasticity [56]. Furthermore, Egr2 may implicate in stimulating iron acquisition in pro-inflammatory conditions [57]. Consequently, we speculated that Egr2 may play a crucial role in cognitive function correlated to mitochondrial iron metabolism. In this study, the WB assay showed that the protein level of ACSL4, COX2, Ferroportin1 and DMT1 was upregulated, and the GPX4 and FTH1 protein level were downregulated after sevoflurane administration, while which were reversed when Egr2 expression was suppressed. Meanwhile, the iron assay showed that sevoflurane administration significantly induced iron overload, and the iron deposition was apparently elevated in hippocampus indicated by Perls' Prussian blue staining.

Collectively, these findings documented that sevoflurane administration reduced the mitochondrial membrane potential, and elevated the mitochondrial membrane-permeability, and further initiated iron dyshomeostasis. These changes facilitated the neuronal dysfunction and eventually resulted in cognitive deficiency, whereas suppressing Egr2 expression partly reversed this pathological process.

Declarations

Funding

This research was supported by the National Natural Science Foundation of China (No.81371214, No.81671063 and No.82001424), the Zhejiang Provincial Natural Science Foundation of China (No. LY16H090008 and No. LQ19H030009), and the Key Program of the Natural Science Foundation of Zhejiang, China (No. LZ19H090003).

Author Contributions

PZ, YRC and GC participated in the design of the experimental protocols. PZ, YRC, SXZ, MF and XYL carried out experimental operation. PZ, YRC, TSL and XY were in charge of the data analysis. PZ, YRC and GC drafted the manuscript. All authors read and approved the final manuscript.

Competing interests

The authors declare that they have no competing interests.

References

1. Needham MJ, Webb CE, Bryden DC: **Postoperative cognitive dysfunction and dementia: what we need to know and do.** *British journal of anaesthesia* 2017, **119:**i115-i125.
2. Kotekar N, Shenkar A, Nagaraj R: **Postoperative cognitive dysfunction - current preventive strategies.** *Clin Interv Aging* 2018, **13:**2267-2273.
3. Rundshagen I: **Postoperative cognitive dysfunction.** *Dtsch Arztebl Int* 2014, **111:**119-125.

4. Ghoneim MM, Block RI: **Clinical, methodological and theoretical issues in the assessment of cognition after anaesthesia and surgery: a review.** *European journal of anaesthesiology* 2012, **29:**409-422.
5. Flores FJ, Hartnack KE, Fath AB, Kim S-E, Wilson MA, Brown EN, Purdon PL: **Thalamocortical synchronization during induction and emergence from propofol-induced unconsciousness.** *Proceedings of the National Academy of Sciences of the United States of America* 2017, **114:**E6660-E6668.
6. Xu L, Hu Y, Huang L, Liu Y, Wang B, Xie L, Hu Z: **The association between attention deficit hyperactivity disorder and general anaesthesia - a narrative review.** *Anaesthesia* 2019, **74:**57-63.
7. Ghatge S, Lee J, Smith I: **Sevoflurane: an ideal agent for adult day-case anesthesia?** *Acta anaesthesiologica Scandinavica* 2003, **47:**917-931.
8. Song SY, Meng XW, Xia Z, Liu H, Zhang J, Chen QC, Liu HY, Ji FH, Peng K: **Cognitive impairment and transcriptomic profile in hippocampus of young mice after multiple neonatal exposures to sevoflurane.**
9. Xu G, Lu H, Dong Y, Shapoval D, Soriano SG, Liu X, Zhang Y, Xie Z: **Coenzyme Q10 reduces sevoflurane-induced cognitive deficiency in young mice.** *British journal of anaesthesia* 2017, **119:**481-491.
10. Liu B, Xia J, Chen Y, Zhang J: **Sevoflurane-Induced Endoplasmic Reticulum Stress Contributes to Neuroapoptosis and BACE-1 Expression in the Developing Brain: The Role of eIF2α.** *Neurotox Res* 2017, **31:**218-229.
11. Xie S-N, Ye H, Li J-F, An L-X: **Sevoflurane neurotoxicity in neonatal rats is related to an increase in the GABA R α1/GABA R α2 ratio.** *Journal of neuroscience research* 2017, **95:**2367-2375.
12. Amrock LG, Starner ML, Murphy KL, Baxter MG: **Long-term effects of single or multiple neonatal sevoflurane exposures on rat hippocampal ultrastructure.** *Anesthesiology* 2015, **122:**87-95.
13. Ji M-H, Qiu L-L, Yang J-J, Zhang H, Sun X-R, Zhu S-H, Li W-Y, Yang J-J: **Pre-administration of curcumin prevents neonatal sevoflurane exposure-induced neurobehavioral abnormalities in mice.** *Neurotoxicology* 2015, **46:**155-164.
14. Li L, Carter J, Gao X, Whitehead J, Tourtellotte WG: **The neuroplasticity-associated arc gene is a direct transcriptional target of early growth response (Egr) transcription factors.** *Molecular and cellular biology* 2005, **25:**10286-10300.
15. DeSteno DA, Schmauss C: **Induction of early growth response gene 2 expression in the forebrain of mice performing an attention-set-shifting task.** *Neuroscience* 2008, **152:**417-428.
16. Hoban AE, Stilling RM, Moloney G, Shanahan F, Dinan TG, Clarke G, Cryan JF: **The microbiome regulates amygdala-dependent fear recall.** *Mol Psychiatry* 2018, **23:**1134-1144.
17. Poirier R, Cheval H, Mailhes C, Charnay P, Davis S, Laroche S: **Paradoxical role of an Egr transcription factor family member, Egr2/Krox20, in learning and memory.** *Front Behav Neurosci* 2007, **1:**6.
18. Paul BT, Manz DH, Torti FM, Torti SV: **Mitochondria and Iron: current questions.** *Expert Rev Hematol* 2017, **10:**65-79.

19. Jang JY, Blum A, Liu J, Finkel T: **The role of mitochondria in aging.** *The Journal of clinical investigation* 2018, **128:**3662-3670.
20. Rivera-Mancía S, Pérez-Neri I, Ríos C, Tristán-López L, Rivera-Espinosa L, Montes S: **The transition metals copper and iron in neurodegenerative diseases.** *Chem Biol Interact* 2010, **186:**184-199.
21. Wessling-Resnick M: **Excess iron: considerations related to development and early growth.** *The American journal of clinical nutrition* 2017, **106:**1600S-1605S.
22. Kim J, Wessling-Resnick M: **Iron and mechanisms of emotional behavior.** *J Nutr Biochem* 2014, **25:**1101-1107.
23. de Lima MNM, Polydoro M, Laranja DC, Bonatto F, Bromberg E, Moreira JCF, Dal-Pizzol F, Schröder N: **Recognition memory impairment and brain oxidative stress induced by postnatal iron administration.** *The European journal of neuroscience* 2005, **21:**2521-2528.
24. Zhong JY, Magnusson KR, Swarts ME, Clendinen CA, Reynolds NC, Moffat SD: **The application of a rodent-based Morris water maze (MWM) protocol to an investigation of age-related differences in human spatial learning.** *Behav Neurosci* 2017, **131:**470-482.
25. Lee J, Venna VR, Durgan DJ, Shi H, Hudobenko J, Putluri N, Petrosino J, McCullough LD, Bryan RM: **Young versus aged microbiota transplants to germ-free mice: increased short-chain fatty acids and improved cognitive performance.** *Gut microbes* 2020.
26. Hales JB, Vincze JL, Reitz NT, Ocampo AC, Leutgeb S, Clark RE: **Recent and remote retrograde memory deficit in rats with medial entorhinal cortex lesions.** *Neurobiol Learn Mem* 2018, **155:**157-163.
27. Ge SX, Son EW, Yao R: **iDEP: an integrated web application for differential expression and pathway analysis of RNA-Seq data.** *BMC bioinformatics* 2018, **19:**534.
28. Kanehisa M, Goto S: **KEGG: kyoto encyclopedia of genes and genomes.** *Nucleic acids research* 2000, **28:**27-30.
29. Szklarczyk D, Franceschini A, Wyder S, Forslund K, Heller D, Huerta-Cepas J, Simonovic M, Roth A, Santos A, Tsafou KP, et al: **STRING v10: protein-protein interaction networks, integrated over the tree of life.** *Nucleic acids research* 2015, **43:**D447-452.
30. Zhang CH, Fan YY, Wang XF, Xiong JY, Tang YY, Gao JQ, Shen Z, Song XH, Zhang JY, Shen Y, et al: **Acidic preconditioning protects against ischemia-induced brain injury.** *Neuroscience letters* 2012, **523:**3-8.
31. Zhou Y-F, Wang Q-X, Zhou H-Y, Chen G: **Autophagy activation prevents sevoflurane-induced neurotoxicity in H4 human neuroglioma cells.** *Acta pharmacologica Sinica* 2016, **37:**580-588.
32. Li C, Zhang Y, Cheng X, Yuan H, Zhu S, Liu J, Wen Q, Xie Y, Liu J, Kroemer G, et al: **PINK1 and PARK2 Suppress Pancreatic Tumorigenesis through Control of Mitochondrial Iron-Mediated Immunometabolism.** *Dev Cell* 2018, **46**.
33. Béïque J-C, Na Y, Kuhl D, Worley PF, Huganir RL: **Arc-dependent synapse-specific homeostatic plasticity.** *Proceedings of the National Academy of Sciences of the United States of America* 2011, **108:**816-821.

34. Greer PL, Hanayama R, Bloodgood BL, Mardinly AR, Lipton DM, Flavell SW, Kim T-K, Griffith EC, Waldon Z, Maehr R, et al: **The Angelman Syndrome protein Ube3A regulates synapse development by ubiquitinating arc.** *Cell* 2010, **140:**704-716.
35. Riess ML, Eells Jt Fau - Kevin LG, Kevin Lg Fau - Camara AKS, Camara Ak Fau - Henry MM, Henry Mm Fau - Stowe DF, Stowe DF: **Attenuation of mitochondrial respiration by sevoflurane in isolated cardiac mitochondria is mediated in part by reactive oxygen species.**
36. Wang ZB, Liu JY, Xu XJ, Mao XY, Zhang W, Zhou HH, Liu ZQ: **Neurodegeneration with brain iron accumulation: Insights into the mitochondria dysregulation.**
37. Kapoor I, Prabhakar H, Mahajan C: **Postoperative Cognitive Dysfunction.** *Indian J Crit Care Med* 2019, **23:**S162-S164.
38. Monk TG, Weldon BC, Garvan CW, Dede DE, van der Aa MT, Heilman KM, Gravenstein JS: **Predictors of cognitive dysfunction after major noncardiac surgery.** *Anesthesiology* 2008, **108:**18-30.
39. Yang C-W, Fuh J-L: **Exposure to general anesthesia and the risk of dementia.** *Journal of pain research* 2015, **8:**711-718.
40. Wei H, Xie Z: **Anesthesia, calcium homeostasis and Alzheimer's disease.** *Curr Alzheimer Res* 2009, **6:**30-35.
41. Haseneder R, Kratzer S, von Meyer L, Eder M, Kochs E, Rammes G: **Isoflurane and sevoflurane dose-dependently impair hippocampal long-term potentiation.** *European journal of pharmacology* 2009, **623:**47-51.
42. Liu Y, Yan J, Sun C, Li G, Li S, Zhang L, Di C, Gan L, Wang Y, Zhou R, et al: **Ameliorating mitochondrial dysfunction restores carbon ion-induced cognitive deficits via co-activation of NRF2 and PINK1 signaling pathway.** *Redox Biol* 2018, **17:**143-157.
43. Hollensworth SB, Shen C, Sim JE, Spitz DR, Wilson GL, LeDoux SP: **Glial cell type-specific responses to menadione-induced oxidative stress.** *Free radical biology & medicine* 2000, **28:**1161-1174.
44. Xu B, Lang L-M, Li S-Z, Guo J-R, Wang J-F, Wang D, Zhang L-P, Yang H-M, Lian S: **Cortisol Excess-Mediated Mitochondrial Damage Induced Hippocampal Neuronal Apoptosis in Mice Following Cold Exposure.** *Cells* 2019, **8**.
45. Voets AM, Huigsloot M, Lindsey PJ, Leenders AM, Koopman WJH, Willems PHGM, Rodenburg RJ, Smeitink JAM, Smeets HJM: **Transcriptional changes in OXPHOS complex I deficiency are related to anti-oxidant pathways and could explain the disturbed calcium homeostasis.** *Biochimica et biophysica acta* 2012, **1822:**1161-1168.
46. Vianna MR, Alonso M, Viola H, Quevedo J, de Paris F, Furman M, de Stein ML, Medina JH, Izquierdo I: **Role of hippocampal signaling pathways in long-term memory formation of a nonassociative learning task in the rat.** *Learning & memory (Cold Spring Harbor, NY)* 2000, **7:**333-340.
47. Lin H-P, Oksuz I, Svaren J, Awatramani R: **Egr2-dependent microRNA-138 is dispensable for peripheral nerve myelination.** *Scientific reports* 2018, **8:**3817.
48. Phelps ED, Sweeney KR, Blader IJ: **Toxoplasma gondii rhoptry discharge correlates with activation of the early growth response 2 host cell transcription factor.** *Infect Immun* 2008, **76:**4703-4712.

49. Peleli M, Ferreira DMS, Tarnawski L, McCann Haworth S, Xuechen L, Zhuge Z, Newton PT, Massart J, Chagin AS, Olofsson PS, et al: **Dietary nitrate attenuates high-fat diet-induced obesity via mechanisms involving higher adipocyte respiration and alterations in inflammatory status.** *Redox Biol* 2020, **28:**101387.
50. Wang J, Pantopoulos K: **Regulation of cellular iron metabolism.** *The Biochemical journal* 2011, **434:**365-381.
51. Singh N, Haldar S, Tripathi AK, Horback K, Wong J, Sharma D, Beserra A, Suda S, Anbalagan C, Dev S, et al: **Brain iron homeostasis: from molecular mechanisms to clinical significance and therapeutic opportunities.** *Antioxidants & redox signaling* 2014, **20:**1324-1363.
52. Hui Y, Wang D, Li W, Zhang L, Jin J, Ma N, Zhou L, Nakajima O, Zhao W, Gao X: **Long-term overexpression of heme oxygenase 1 promotes tau aggregation in mouse brain by inducing tau phosphorylation.** *Journal of Alzheimer's disease : JAD* 2011, **26:**299-313.
53. Wu J, Yang J-J, Cao Y, Li H, Zhao H, Yang S, Li K: **Iron overload contributes to general anaesthesia-induced neurotoxicity and cognitive deficits.** *Journal of neuroinflammation* 2020, **17:**110.
54. Eaton JW, Qian M: **Molecular bases of cellular iron toxicity.** *Free radical biology & medicine* 2002, **32:**833-840.
55. Richardson DR, Lane DJR, Becker EM, Huang MLH, Whitnall M, Suryo Rahmanto Y, Sheftel AD, Ponka P: **Mitochondrial iron trafficking and the integration of iron metabolism between the mitochondrion and cytosol.** *Proceedings of the National Academy of Sciences of the United States of America* 2010, **107:**10775-10782.
56. Rosa P, Zerbinati C, Crestini A, Canudas A-M, Ragona G, Confaloni A, Iuliano L, Calogero A: **Heme Oxygenase-1 and Brain Oxysterols Metabolism Are Linked to Egr-1 Expression in Aged Mice Cortex, but Not in Hippocampus.** *Frontiers in aging neuroscience* 2018, **10:**363.
57. Cellier MFM: **Developmental Control of NRAMP1 (SLC11A1) Expression in Professional Phagocytes.** *Biology (Basel)* 2017, **6**.

Table

Table. 1 Effects of sevoflurane exposure on physiological parameters of arterial blood gas analysis of neonatal mice

		Arterial Blood Gas			
	n	pH	$PaCO_2$, mmHg	PaO_2, mmHg	SaO_2, %
Ctrl group	10	7.32±0.06	26.8±4.1	98.1±4.8	95.4±1.1
SEV group	10	7.46±0.04	27.3±3.9	81.4±6.9	95.4±0.9

There is no significant difference in Ph, PaCO2, PaO2, Glucose and SaO2 between the groups.

PaCO2 = arterial carbon dioxide tension; PaO2 = arterial oxygen tension; SaO2 = arterial oxygen saturation.

Figures

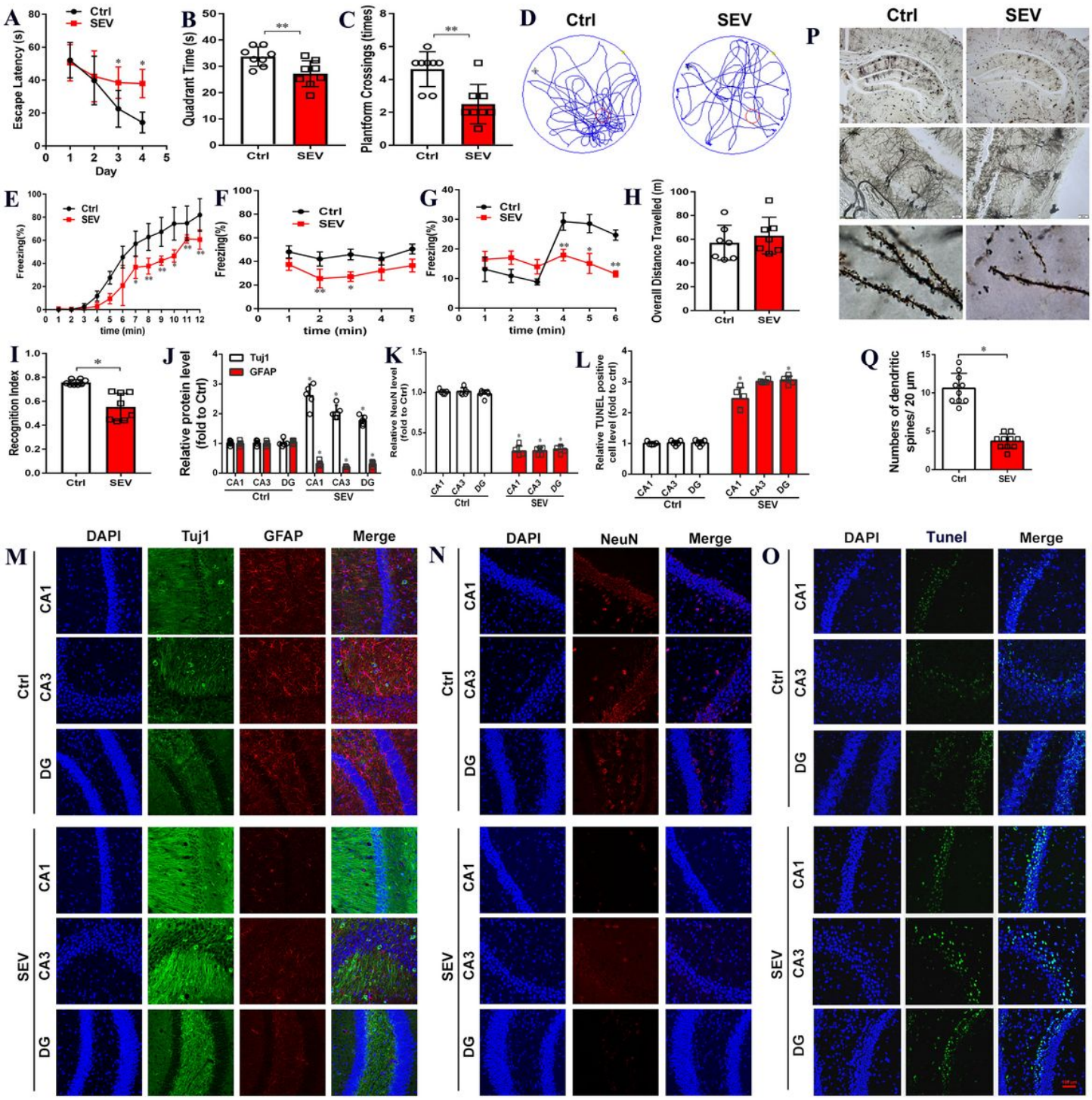

Figure 1

Sevoflurane Exposures induced Cognitive Impairment accompanying by neuronal death and reducing synapse formation in hippocampus (A-D) Morris water maze test including the time course of escape latency, the time spent in the target quadrant and the times crossing the hidden platform, and moving track; (E-G) Freezing behavior detected by fear condition test; (H, I) Novel object recognition comprising of the overall distance of traveling and the recognition index; (J-L, Q) Quantitative results for Tuj1, GFAP, NeuN, Tunel staining, and Golgi-Cox staining, respectively; (M, N) Expression of neuron-specific Tuj1 and

NeuN in hippocampus indicated by immunofluorescent staining; (O) Cell apoptosis detection by Alexa Fluor 488 reagent; (P) Representative images of Golgi-Cox staining sections in hippocampus. Scar bar = 100 μm, applied in Fig M-O. *P < 0.05, ** P < 0.01, Ctrl VS SEV.

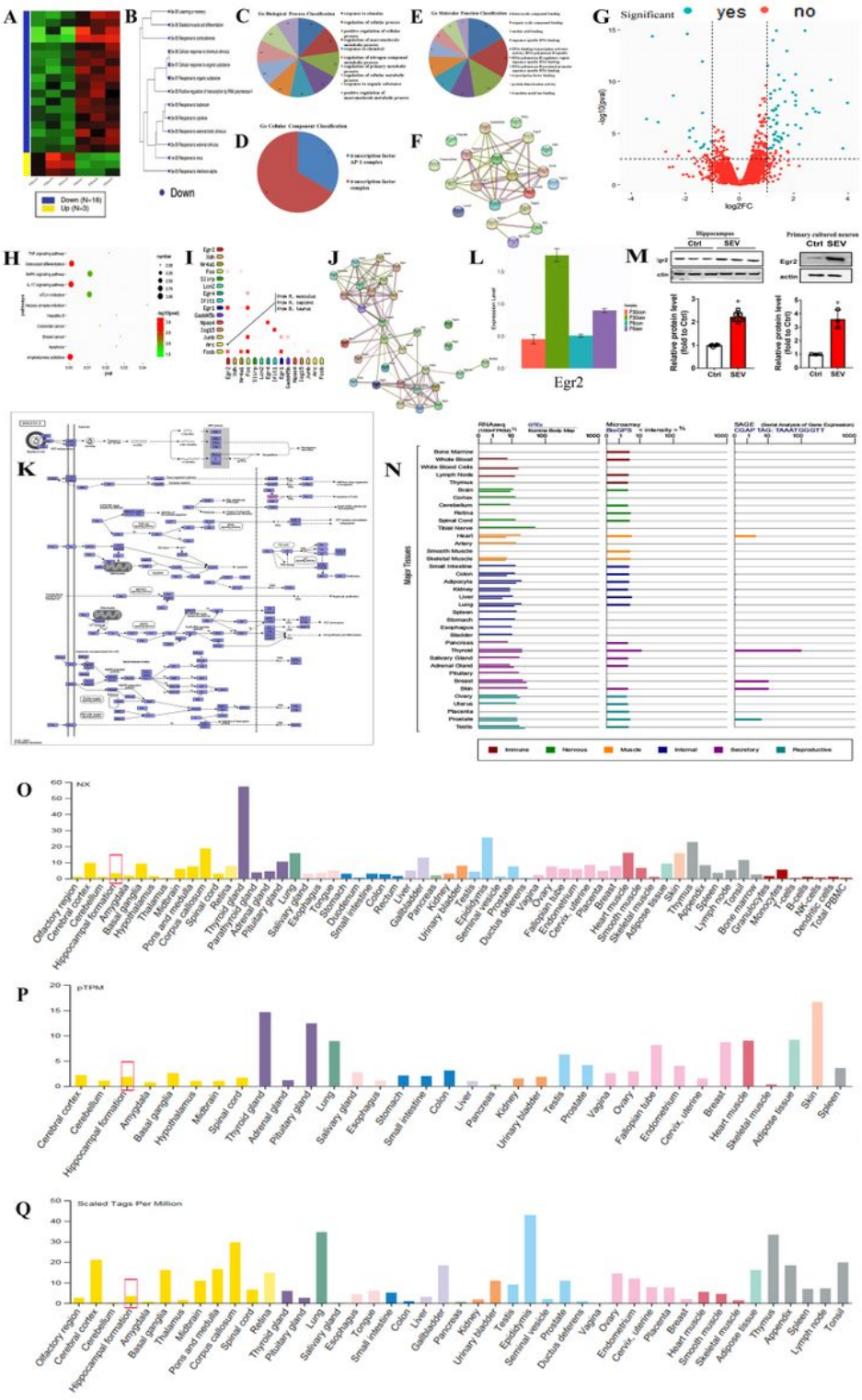

Figure 2

Bioinformatics analysis indicated that Sevoflurane administration resulted in the Egr2 expression significantly upregulated (A-B) Cluster analysis of DEGs for heat map and dendrogram; (C-F) GO function

analysis including biological process (BP), cellular component (CC), and molecular function (MF), and the PPI network construction; (G) The volcano plot for displaying the distribution of DEGs; (H) Bubble plot showed the related signal pathways based on GO analysis; x-axis represents the P value and y-axis descript the enrichment components. The area of the circle is proportional to the number of genes assigned to the term and the color accords with the P value; (I) Gene coexpression was identified by String tools; (J) PPI network construction for mediating cognitive function and mitochondrial function; (K) The signal pathway based on KEGG Pathway Database; (L) The expression level of Egr2 obtained from RNA-Seq; (M) WB assay for detecting the relative protein level of Egr2 in animal hippocampus and primary cultured neuron, respectively; (N-Q) The Egr2 expression in different tissues resulted from Genecards database and The Human Protein Atlas website. *P < 0.05, Ctrl VS SEV.

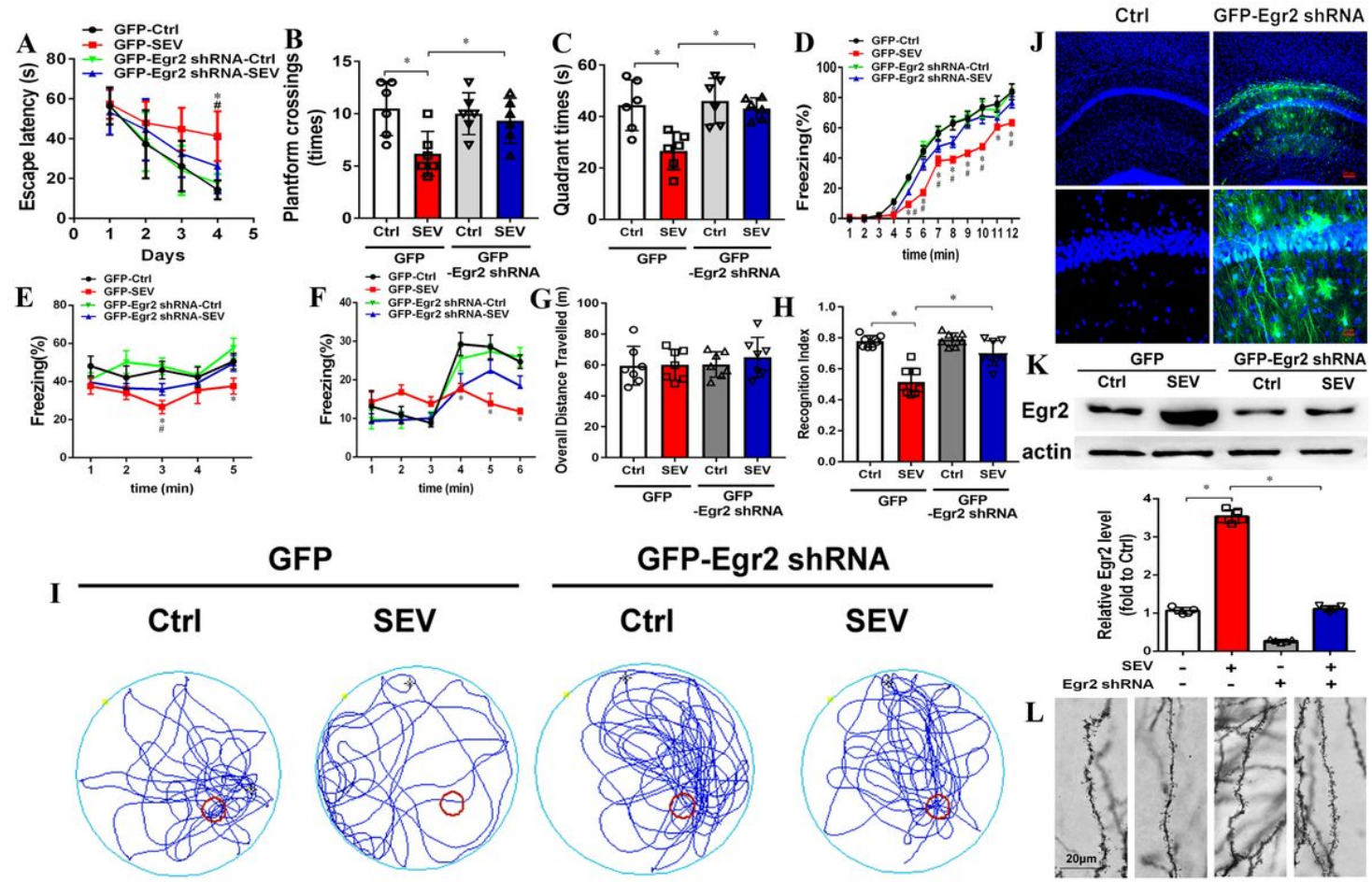

Figure 3

Egr2 downregulation alleviated the cognitive deficits induced by sevoflurane administration (A-C, I) Morris water maze test consisting of the time course of escape latency, the times crossing the hidden platform, the time spent in the target quadrant, and motion trail; (D-F) Freezing behavior detected by fear condition test; (G, H) Novel object recognition comprising of the overall distance of traveling and the recognition index; (J) The transfection of recombinant adeno-associated virus (AAV) in the hippocampus by intracerebroventricular injection; (K) WB assay for detecting the Egr2 protein level; (L) Representative

images of Golgi-Cox staining sections in hippocampus. Scar bar = 100/30 μm, applied in Fig J; Scar bar = 20 μm in Fig L. *P < 0.05, GFP-Ctrl VS GFP-SEV; #P < 0.05, GFP-Egr2 shRNA-SEV VS GFP-SEV.

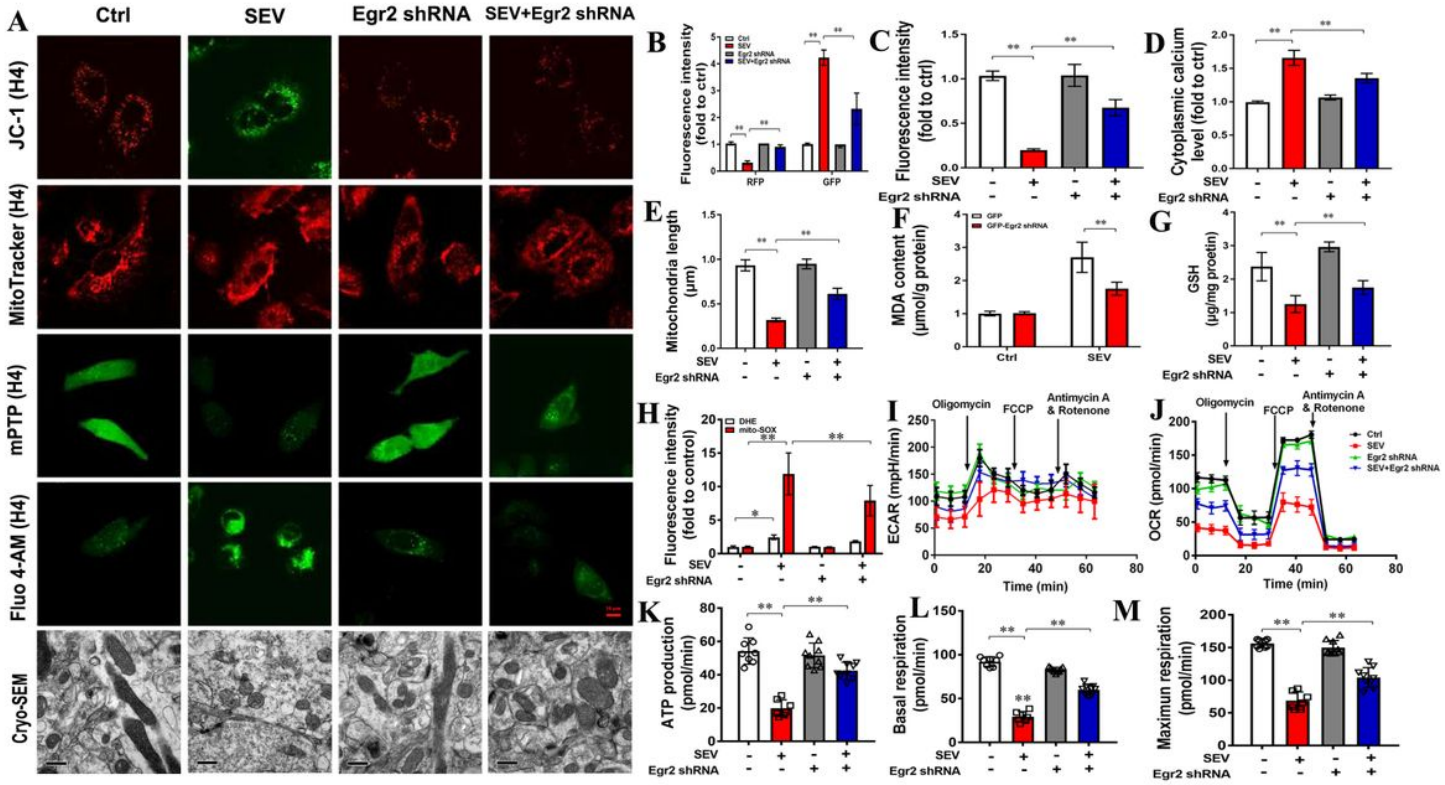

Figure 4

Egr2 downregulation partly improved mitochondrial dysfunction following Sevoflurane administration (A-D) Immunofluorescent staining by using JC-1 probe, MitoTracker staining, Mitochondrial permeability transition pore assay, and Fluo 4-AM calcium indicators to investigate mitochondrial membrane potential, morphology and membrane permeability, and cytoplasm calcium levels, respectively; (A, E) Cryo-electron microscopy observation and the mitochondrial length calculation; (F, G) Detection for the level of MDA and GSH; (H) The DHE and mito-SOX staining for measuring the level of intracellular and mitochondrial ROS; (I-M) Aerobic respiration and anaerobic glycolysis detection including ECAR and OCR assay. Scar bar = 10 μm, applied in Fig A.*P < 0.05, ** P < 0.01.

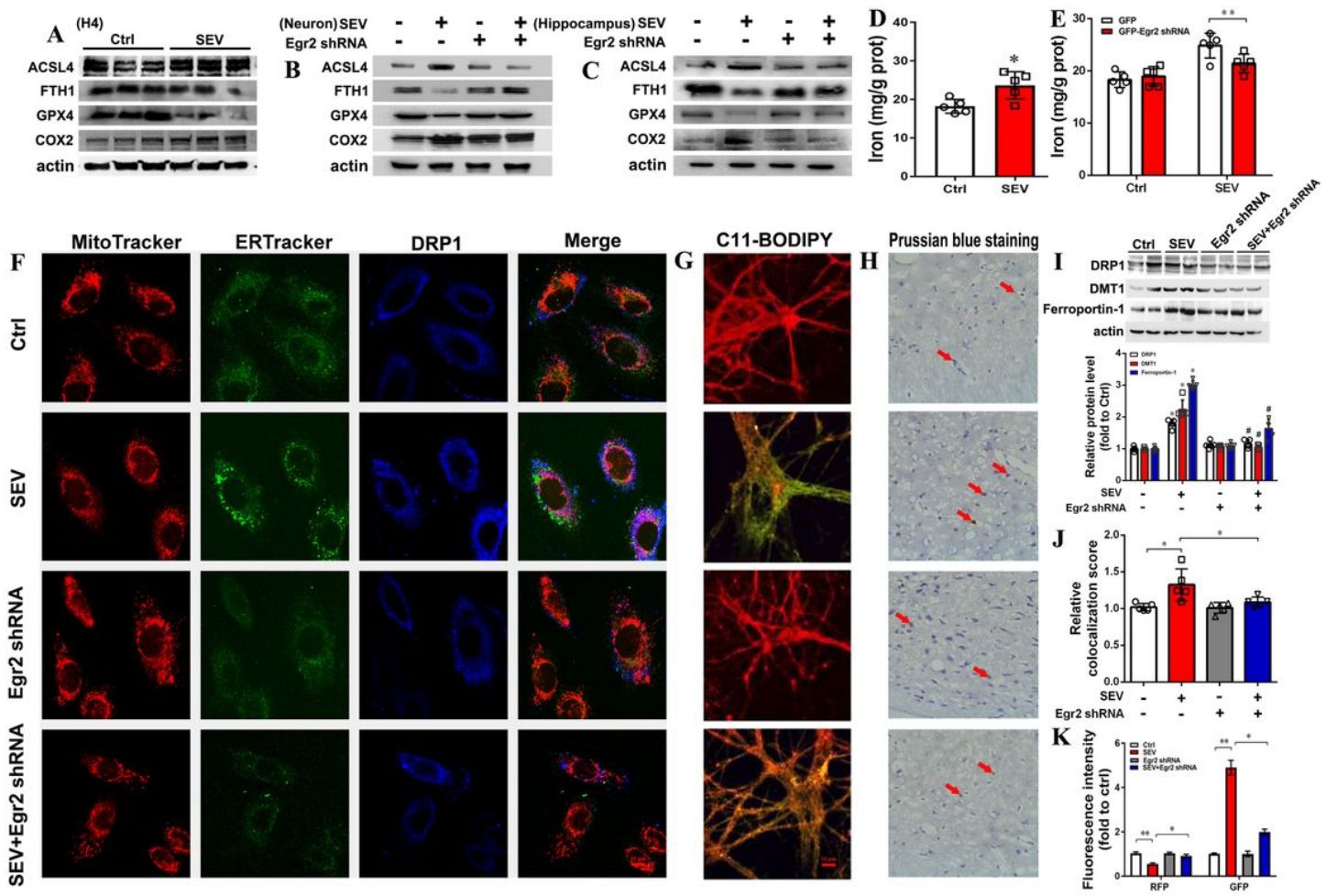

Figure 5

Egr2 downregulation alleviates iron overload-induced ER-mediated mitochondrial fission in hippocampal primary neurons (A-C) WB assay for detecting iron metabolism-related proteins; (D, E) Iron content detection; (F) Immunofluorescent staining for detecting the correlation between Egr2 expression and iron overload-induced mitochondrial fission; (G, K) C11-BODIPY staining for determining the level of lipid peroxidation; (H) Prussian blue staining for detecting iron deposition; (I) WB assay for detecting iron metabolism and mitochondrial fission-related proteins; (J) Manders' overlap coefficient (MOC) was calculated to determine the degree of colocalization. Scar bar = 10 μm, applied in Fig F, G. Red arrow indicates the positive cells of Prussian blue staining. *P < 0.05, GFP-Ctrl VS GFP-SEV; #P < 0.05, GFP-Egr2 shRNA-SEV VS GFP-SEV.

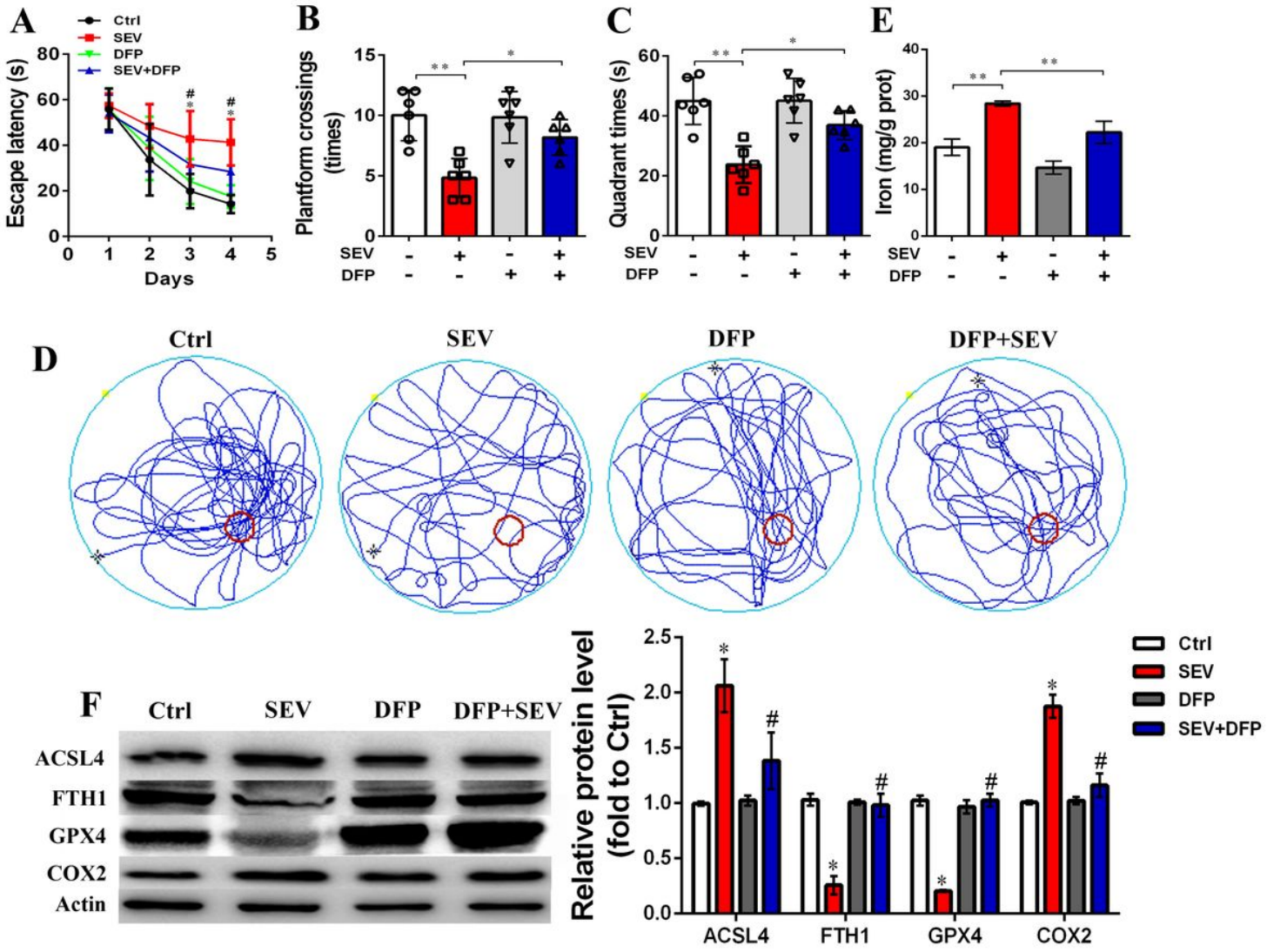

Figure 6

The behavioral performance was effectively improved after deferiprone administration (A-D) Morris water maze test consisting of the time course of escape latency, the times crossing the hidden platform, the time spent in the target quadrant, and motion trail; (E) Iron content detection; (F) WB assay for detecting iron metabolism-related proteins. *P < 0.05, Ctrl VS SEV; #P < 0.05, SEV VS SEV+DFP.

Supplementary Files

This is a list of supplementary files associated with this preprint. Click to download.

- FigureS.jpg
- Supplementarymaterial.docx
- TableS1.csv
- TableS2.csv

- TableS3.csv
- TableS4.csv
- TableS5.csv
- TableS6.csv